

1 Ina Lunar Irregular Mare Patch (IMP) **Mission Concepts: Distinguishing**
2 **Between Ancient and Modern Volcanism Models**

3
4 Le Qiao^{1,2}, James W. Head³, Lionel Wilson⁴, and Zongcheng Ling²

5
6 Abstract

7 The Ina Irregular Mare Patch (IMP), a $\sim 2 \times 3$ km summit depression on an
8 ancient ~ 22 km diameter shield volcano, displays two very enigmatic
9 units: 1) dozens of dark convex-upward mounds, 2) a very rough,
10 optically immature floor unit, with very sharp morphologic contacts
11 between the two. Controversy surrounds the age interpretation of Ina:
12 superposed impact crater size-frequency distributions (CSFD) suggest an
13 age of ~ 33 Ma, consistent with the presence of sharp contacts between
14 the units, and indicating that mare volcanism continues to today. Models
15 of the terminal stages of volcano summit pit crater activity suggest an
16 age coincident with the building of the shield, ~ 3.5 Ga; these models
17 interpret the CSFD age and sharp contacts to be due to an extremely
18 porous lava lake floor, and extrusion and solidification of magmatic
19 foams. We present robotic-human exploration mission concepts designed to
20 resolve this critical issue for lunar thermal evolution.

21
22
23
24
25
26
27

¹ Corresponding author leqiao.geo@gmail.com

² Shandong Key Laboratory of Optical Astronomy and Solar-Terrestrial Environment, School of Space Science and Physics, Institute of Space Sciences, Shandong University, Weihai, Shandong, 264209, China.

³ Department of Earth, Environmental and Planetary Sciences, Brown University, Providence, RI 02912, USA.

⁴ Lancaster Environment Centre, Lancaster University, Lancaster LA1 4YQ, UK.

1. Introduction and Background

While examining the high-resolution orbital photographs taken by the Apollo 15 crew in August 1971, Whitaker (1972) noted a very unusual and enigmatic depression feature (18.66°N, 5.30°E), ~3 × 2 km in size, with about half of the depression floor covered with blobs of mare materials with an appearance similar to "dirty mercury." Located in a small mare in the central portion of the nearside Moon, the feature was informally named "D-Caldera" (Cernan et al. 1972; El-Baz 1973; Evans & El-Baz 1973) and then formally known as Ina (Defense Mapping Agency 1974; Strain & El-Baz 1980) (Figures 1 and 2). Its peculiar shape and interior structures intrigued many Apollo program scientists (El-Baz 1972, 1973; Whitaker 1972). Soon after its discovery, a special orbital visual observation effort for the Ina feature was planned during the Apollo 17 mission in December 1972. The Command Module Pilot (CMP) Ronald E. Evans then presented remarkable observations of the Ina/D-Caldera feature from lunar orbit (Cernan et al. 1972):

"[The] D-Caldera is sure a depression. Like nothing I've ever seen before ... At this point, you get a dark tan, a mare-type material. And then it is a light gray down in the D-Caldera itself ... And then it has got bumps that stick up, and the bumps themselves are the light tan material... And down between the bumps [is] a rough, blocky, gray material." (CMP, revolution 28; words in brackets are not original)

"The pictures confirm a topographic rise around the D-Caldera, just a slight one, and it is about half the width of the D-[Caldera]. And it seems to be a raised, flat rim around it. The color of the raised bumps down in the D-Caldera are the same as the surrounding material. The bumps that are raised up are smooth looking and ... the part of the depression, anyhow, is a light bluish gray." (CMP, revolution 36)

"Down in the caldera, the gray blocky-type of stuff [looks like] water drops on a surface ... But it would leave a depression due to a surface tension ... And then you have little bubbles that float across there ... I could not see a light-colored annulus [around D-Caldera] ... There is nothing surrounding D-Caldera that looks like the silver, gray material that has depressed. The little bumps in D-Caldera are the same color and the same smoothness as the mare material surrounding the area." (CMD, revolution 40)

In addition, the Apollo 17 mission also obtained a sequence of orbital photographs with both color and black-white film. Many Apollo 17 photographs were taken at very low-Sun illumination conditions, which exaggerated surface object shadow patterns and thus significantly enhanced surface morphologic detectability. Geological investigations of these photographs identified Ina

71 as a summit vent depression atop a small extrusive lava dome, with a raised
72 rim "collar" feature (El-Baz 1973; Evans & El-Baz 1973; Strain & El-Baz 1980;
73 Figure 1). The interior of Ina is characterized by various terrain types,
74 including (1) dozens of disconnected blister-like smooth textured mounds, (2)
75 a hummocky-textured floor unit, which is further divided into two albedo
76 portions, light-colored and dark-colored (the latter occurs predominantly
77 along the eastern edge of the Ina floor), and (3) bright materials found
78 around the raised mounds and along the edges of the floor (Figure 2). On the
79 basis of these observations and comparison with terrestrial volcanic analogues
80 (for instance, lava pillars in northern Iceland at Dimmuborgir, Strain & El-
81 Baz 1980), most or all of the morphologies associated with Ina were described
82 to be volcanic in origin (El-Baz 1972, 1973; Evans & El-Baz 1973; Strain & El-
83 Baz 1980). Specifically, the hummocky floor terrains were interpreted as
84 solidified lava lake crust and pyroclastic deposits, and the mounds were
85 thought to be formed as discrete lava extrusions, among the youngest volcanic
86 features on the Moon (El-Baz 1972, 1973; Evans & El-Baz 1973; Strain & El-Baz
87 1980).

88 The international fleet of spacecraft launched to the Moon during the past
89 decade has obtained unprecedented high-resolution imagery data for the nearly
90 global lunar surface, especially the **Lunar Reconnaissance Orbiter** Narrow Angle
91 Cameras (LROC NAC) onboard NASA's Lunar Reconnaissance Orbiter, which has
92 continuously mapped the lunar surface with a pixel size of $\sim 0.5\text{--}2$ m (from the
93 nominal 50 km orbit) since 2009 (Robinson et al. 2010). Survey of the LROC NAC
94 imagery sets found many lunar surface features resembling Ina (Stooke 2012;
95 Braden et al. 2014; Zhang et al. 2018). In particular, Braden et al. (2014)
96 conducted a global search of NAC data and catalogued a total of 70 small mare
97 features with Ina-like characteristics, and termed them irregular mare patches
98 (IMPs). Integrating analyses from morphology, topography, stratigraphy, and
99 spectroscopy of Ina and other IMP features led Braden et al. (2014) to suggest
100 the lower hummocky terrains to be a collapsed volcanic caldera floor or
101 fragmented lava lake crust, and the stratigraphically higher mounds to be
102 terminal-stage lava extrusions (Figure 3). Braden et al. (2014) also
103 investigated the size-frequency distribution of impact craters (CSFD)
104 superposed on the mound terrains at the three largest IMPs (Ina, Sosigenes,
105 and Cauchy 5), and found that they were all dated to be younger than 100 Ma.
106 These ages implied significant prolongation of the lifetime of lunar volcanism
107 from the youngest previously established ~ 1 Ga ago (e.g., Hiesinger et al.
108 2011; Morota et al. 2011) to geologically very recent, which, if confirmed,
109 would raise a host of questions concerning the correctness of current models
110 of lunar thermal and magmatic evolutions (e.g., Head & Wilson 1992; Shearer et
111 al. 2006; Ziethe et al. 2009).

112 In addition to the geologically very recent volcanic eruption model,
113 various alternative scenarios to account for the characteristics, age and
114 origin of Ina/IMPs have been introduced (Table 1). These include:

115 (1) Sublimation-induced high reflectance of the floor terrains (Whitaker
116 1972).

117 (2) Exposure of underlying ancient (>3.5 Ga) mare deposits through the
118 removal of the surface regolith layer by sudden out-gassing of deep juvenile
119 volatiles within the past 10 Ma (Schultz et al. 2006).

120 (3) Lava flow inflation (mounds) and subsequent lava breakout (floor
121 hummocky terrains) (Garry et al. 2012).

122 (4) Explosive volcanic eruptions and the resultant deposition of fine-
123 grained, block-free pyroclastics (Carter et al. 2013; note that this model is
124 proposed for the Cauchy 5 IMP occurrence, one of the three dated young IMPs
125 (~58 Ma; Braden et al. 2014), not specifically for Ina). A compilation of
126 these previously-proposed scenarios and the resultant deposits for lunar IMPs
127 can be found in Qiao et al. (2020a), and an evaluation of some of these models
128 was presented in Qiao et al. (2018).

129 (5) Formation of Ina in the terminal stages of the associated ancient
130 shield volcano, with the unusual characteristics and age attributed to late
131 stage, magmatic volatile-rich lava lake activity and the resulting macro- and
132 micro-vesicular substrate properties (Qiao et al. 2017, 2018, 2019, 2020a,
133 2020b).

134 Following the comprehensive initial work by Braden et al. (2014), an
135 updated catalog of the entire IMP population was compiled and comprehensive
136 geological analyses of several representative IMPs including Ina were
137 undertaken by Qiao et al. (2017, 2018, 2019, 2020a, 2020b). This provided more
138 detail to this interpretation for the emplacement mechanism and age of Ina and
139 other lunar IMPs. Qiao et al. (2020a) presented an updated inventory of 91 IMP
140 occurrences by synthesizing previous IMP identification results. By
141 documenting the detailed geological context information for each catalogued
142 IMP feature, Qiao et al. (2020a) found that the modes of occurrence of the
143 population of lunar IMPs could be classified into two major groups: (1) pit
144 crater environment (or closed environment), in which the IMPs are contained
145 within volcanic pits, for instance, the summit calderas of small shield
146 volcanos, volcanic dike-tip rilles, or endogenetic pit crater chains, and (2)
147 mare flow environment (or open environment), in which the IMPs are simply
148 emplaced on typical basaltic mare deposits, rather than being contained within
149 a depression (Figure 4). One of the largest IMPs, Cauchy 5 in eastern Mare
150 Tranquillitatis, offers a unique hybrid example of the two IMP types: a large
151 pit crater-type IMP on the shield summit vent floor and hundreds of small
152 mare-type IMPs on the shield flanks (Qiao et al. 2020b). This hybrid IMP
153 provides an excellent opportunity to assess the genetic relationship between
154 the two IMP sub-types. Qiao et al. (2017, 2018, 2019) analyzed two of the

155 largest IMPs of pit crater-type, Ina and Sosigenes in western Mare
156 Tranquillitatis, and proposed that the range of unusual geomorphologies and
157 textures of the interior terrains of the largest lunar IMPs within pit craters
158 can be explained as being due to lava lake activity involving highly
159 vesicular/bubble-rich magma extrusion during the waning-stage evolution of a
160 dike-tip pit crater, contemporaneously with the background mare basalts
161 emplaced more than 3 Ga ago.

162 In this scenario, the hummocky and blocky floor terrains were described as
163 a chilled lava lake crust, and the raised mounds were interpreted as final-
164 stage extrusions of viscous magma with an extreme vesicularity, up to ~95%
165 (magmatic foams) (Figure 4a). The unusual substrate characteristics of the
166 final deposits, abundant macro- and micro-vesicularity for the floor terrains,
167 and substantial micro-vesicularity for the raised mounds, were interpreted to
168 dramatically modify the nature of post-emplacment surface modification
169 processes, including impact cratering, regolith development and accumulation,
170 erosion/disruption of topography, and space weathering, generating the range
171 of highly unusual observed characteristics of Ina and leading to the
172 anomalously young CSFD model ages reported by Braden et al. (2014). Using the
173 hybrid geological relationships displayed at the Cauchy 5 IMP, Qiao et al.
174 (2020b) concluded that the small mare-type IMPs were basically formed by a
175 similar mechanism to that of the large pit crater-type IMPs, but in a
176 different geologic settings (overflow on the rim and flank of the small mare
177 shield volcano). In a non-shield volcano mare flow environment, the extruded
178 highly vesicular magma foams, instead of being contained within a depression
179 crater, would simply overflow beyond the vent rim and be emplaced on the
180 adjacent exterior mare surface as thin foamy lava flows (lava flow Phase 4a of
181 the eruption model of Wilson & Head 2018). Post-flow-emplacment impact events
182 were interpreted to cause collapse in the void-rich flows, exposing the rough
183 and coherent interiors of the foamy flows, as observed at many small mare-type
184 IMPs (Figure 4b).

185 This scenario of waning-stage two-phase lava lake activity and magmatic
186 foam extrusion is supported by a range of observations (Carter et al. 2013;
187 Elder et al. 2017; Qiao et al. 2019, 2020b), including (1) the spatial density
188 disparity of superposed impact craters between the interiors of IMPs (both
189 floor and mound units) and the surrounding mare surfaces, (2) the
190 unconsolidated substrate nature of the Ina mounds derived from Diviner
191 thermophysical measurements, (3) the fine-grained and block-free nature of the
192 small mare-type IMP materials from Arecibo radar mapping data (for Cauchy 5),
193 and (4) the high reflectance and optical immaturity of the IMP deposits. The
194 waning-stage magmatic foam eruption scenario is further supported by recent
195 theoretical assessments of magma ascent and eruption in the final phases of
196 activity in volcanic pit craters/vents (Wilson & Head 2017b) and lava flows
197 (Wilson & Head 2017a, 2018; Head & Wilson 2017). These authors predicted that,

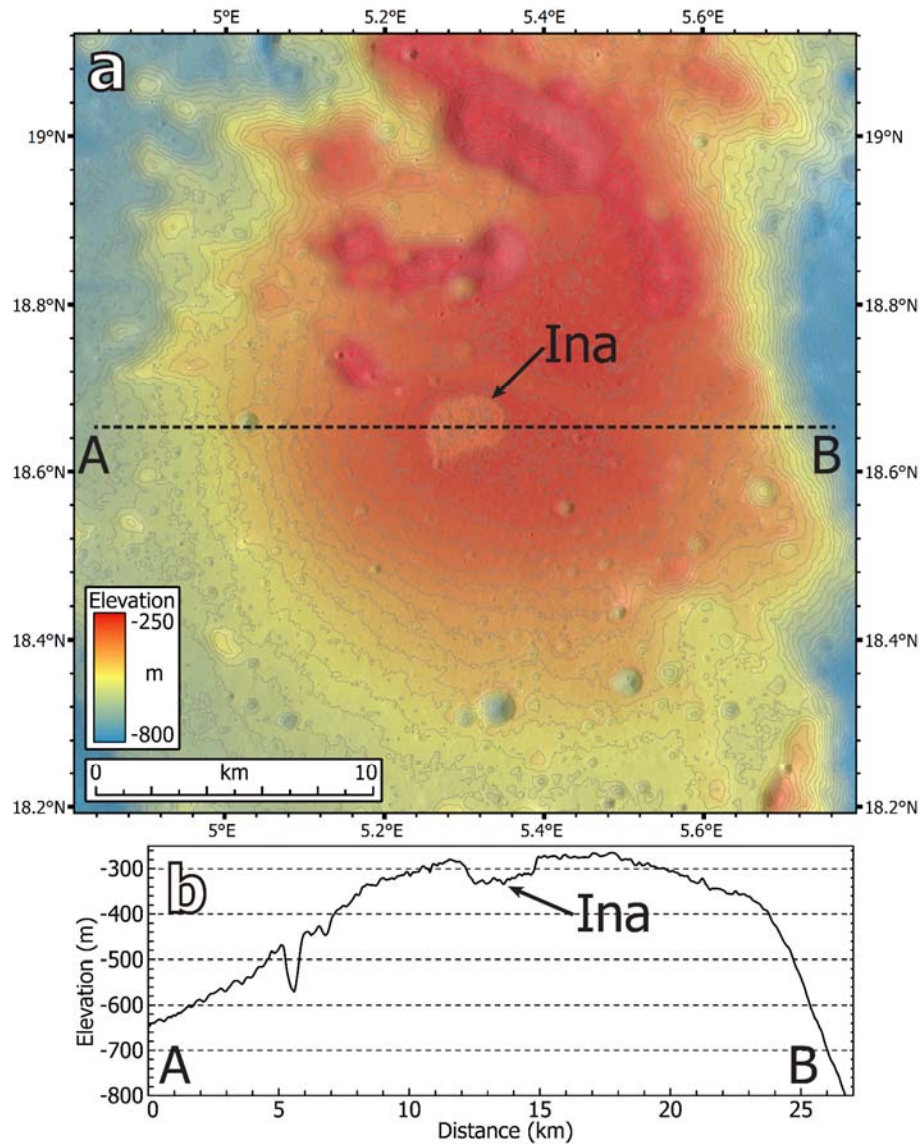
198 during the late-stage activity of lava lakes and fissure eruptions, the magma
199 ascent rate decreased greatly, and shallow gas exsolution in the dike produced
200 highly vesicular magmatic foams. Final-stage dike stress relaxation and dike
201 closure would slowly squeeze the foamy magma out of the dike, cracking the
202 partly solidified lava lake floor, and extruding the convex-upward mounds.

203 In summary, hypotheses for the origin of Ina can be subdivided into two
204 categories (Table 1):

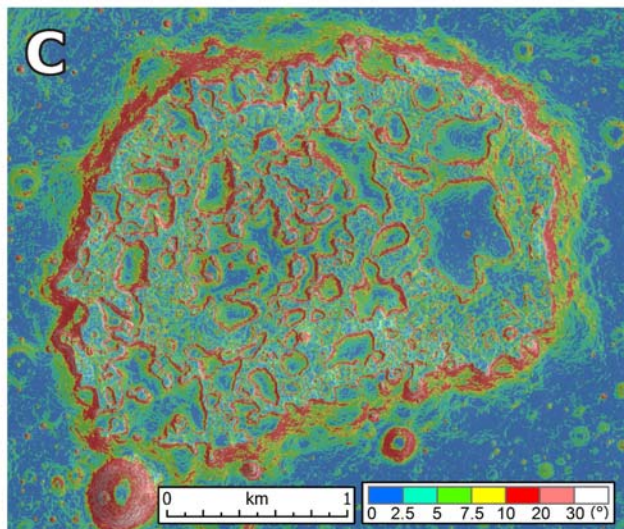
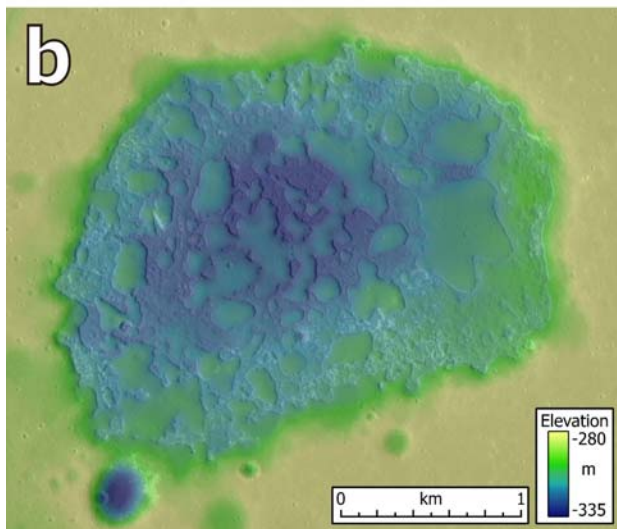
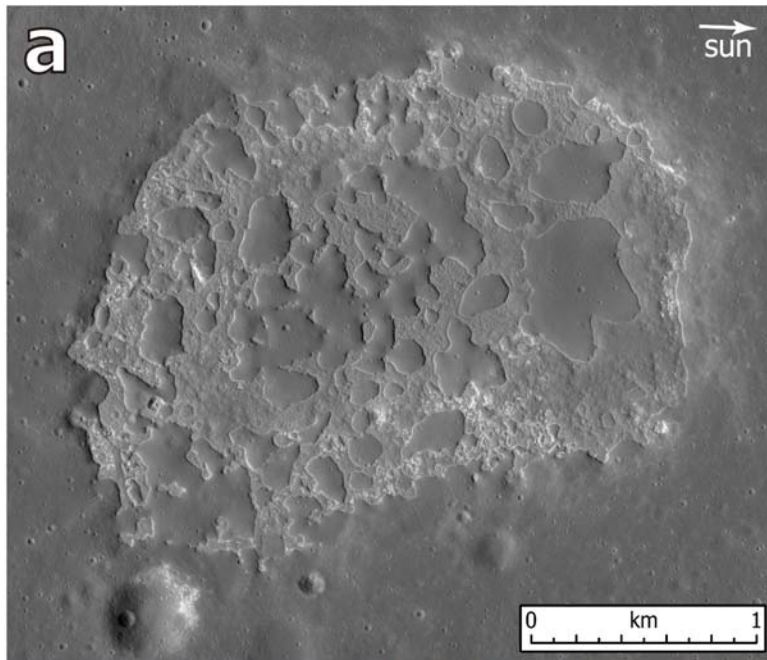
205 (1) Formation age: (a) Geologically extremely young, as indicated by the
206 CSFD ages of ~33 Ma, optical immaturity, and sharp contacts; (b) Geologically
207 ancient, coincident with the ~3.5 Ga age of the surrounding shield volcano,
208 with other factors explained by unusual substrate characteristics; c) Hybrid,
209 geologically old, but rejuvenated by recent activity (outgassing).

210 (2) Setting and mode of emplacement: (a) Formation in the summit pit
211 crater of an ancient shield volcano; (b) Formation in the summit pit crater of
212 an ancient shield volcano, but due to magmatic activity ~3.4 billion years
213 later; (c) Formation by flow inflation processes in a summit pit crater; (d)
214 Formation by late stage volatile exsolution processes in the waning stages of
215 an ancient shield volcano summit vent; (e) Formation by recent deep gas
216 release processes in an ancient shield volcano summit pit crater.

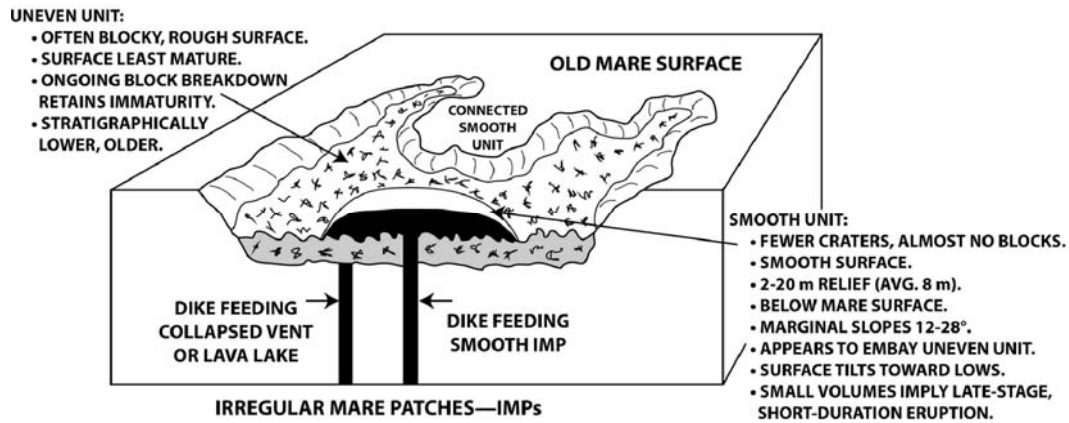
217



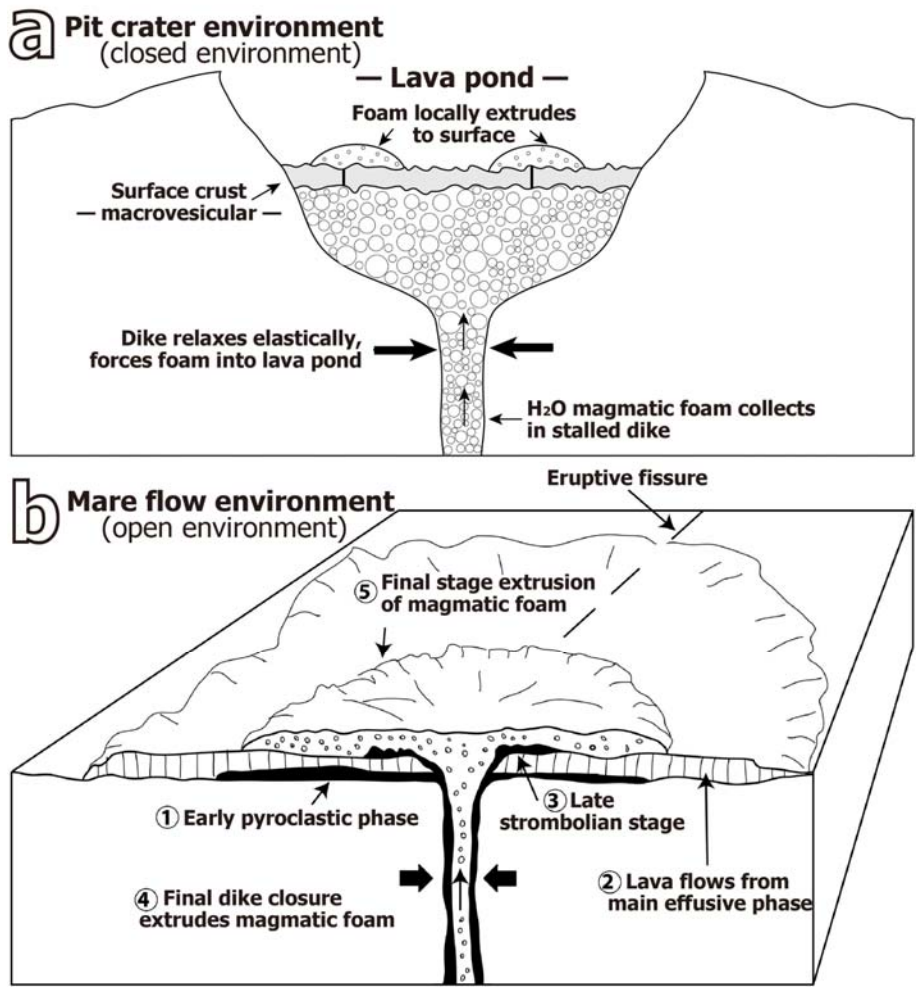
218
 219 **Figure 1.** Location and general setting of Ina pit crater. (a) SLDEM2015
 220 topography of the mare surface surrounding Ina, overlain on Kaguya TC evening
 221 mosaic, 25 m-contour interval and (b) a west-east (A-B) topographic profile
 222 across the Ina shield and summit pit crater, derived from SLDEM2015
 223 topography.
 224



225
 226 **Figure 2.** Ina interior imagery, topographic and slope maps. (a) LROC NAC image
 227 (frame M119815703, 0.48 m/pixel, $\sim 56^\circ$ incidence angle), (b) LROC NAC DTM
 228 topography (2 m/pixel) overlain on NAC image M119815703, (c) NAC DTM-derived
 229 slope (6 m baseline) map overlain on LROC NAC M119815703. **The solar**
 230 **illumination direction is indicated by the white arrow in panel a.**
 231



232
 233 **Figure 3.** Block diagram for the major structures and characteristics of Ina
 234 pit crater, and their mode of emplacement as interpreted by Braden et al.
 235 (2014), in which the uneven floor units represent fragmented lava lake crust
 236 and the mounds are interpreted to be geologically very recent lava extrusions
 237 (<100 Ma), in contrast to the surrounding very ancient mare shield deposits
 238 (~3.5 Ga) (from Head & Wilson 2017).
 239



241 **Figure 4.** Models for late stage foam-rich mare basalt extrusions in (a) pit
 242 craters and (b) unconfined fissure mare foam flow environments (from Wilson &
 243 Head 2017b). (a) Magmatic processes in the dike-tip and summit vent during the
 244 final phases of a small lunar shield-building eruption (e.g., the shield
 245 underlying Ina pit crater); shallow gas exsolution to produce very vesicular
 246 magmatic foams in the dike-tip and vent floor lava lake, fracturing of the
 247 chilled and brittle lava lake crust, and squeeze-ups of the highly foamy lavas
 248 to form bulbous-shaped mounds. (b) Sequence of processes operating in a mare
 249 flow eruption from a fissure vent. Similar magmatic processes to the pit
 250 crater settings (a) are also illustrated here, but due to the lack of a
 251 confining dike-tip pit crater/vent, the highly vesicular foamy lava extrudes
 252 as a broader and thin lava flow. Post-emplacement impacts into these
 253 solidified void-rich lava flows produce many of the small-scale IMPs observed
 254 in lunar maria (Braden et al. 2014; Qiao et al. 2020a).

255
 256
 257

Table 1
 Theories for the Origin and Age of Ina/IMPs.

Ina/IMP origin theory	Formation age	Mode of emplacement	Reference
Sublimation	Not provided	Mounds: mare-like deposits; floor terrain: possible sublimates.	Whitaker 1972
Small lava intrusions associated with a mare dome	Among the youngest lunar volcanism, but specific age not provided	Entire Ina feature: small shield volcano summit caldera; mounds: small volcanic eruptions.	El-Baz 1972, 1973; Strain & El-Baz 1980
Gas release- induced surface regolith removal	Surface exposure age: <10 Ma; Crystallization age: >3.5 Ga	Exposure of buried ancient mare basalts by out-gassing.	Schultz et al. 2006
Lava flow inflation	Not provided	Mounds: inflated lava flows; floor hummocky units: lava breakouts.	Garry et al. 2012
Small basaltic eruptions	<100 Ma	Mounds: small lava extrusions; floor units: lava pond crust.	Braden 2013; Braden et al. 2014

Pyroclastic eruption (proposed only for Cauchy 5 IMP, not for Ina)	Not provided	Pyroclastic deposits.	Carter et al. 2013
Lava lake processes and magmatic foam extrusion	~3.5 Ga	Floor units: solidified lava lake crust; mounds: solidified magmatic foams.	Qiao et al. 2017, 2018, 2019, 2020a, 2020b; Wilson & Head 2017b.

258

259 **2. Significance of the Age and Origin of Ina: The Thermal Evolution of**
 260 **the Moon**

261 While Ina/IMPs are now generally considered to be volcanic in origin, the
 262 specific formation mechanism is still highly controversial (Table 1). One of
 263 the most contentious issues concerning Ina's origin is its emplacement age,
 264 especially between the geologically very recent (<0.1 Ga) small basaltic
 265 eruption model (Braden et al. 2014) and the ancient (>3 Ga) magmatic foam
 266 extrusion hypothesis (Qiao et al. 2017, 2018, 2019, 2020a, 2020b; Wilson &
 267 Head 2017b). On the basis of (1) the physical volcanological study of final-
 268 stage eruption processes and volatile exsolution patterns, and (2) the
 269 detailed geological characterization of Ina's interior units, Qiao et al.
 270 (2017, 2018, 2019, 2020a, 2020b) and Wilson and Head (2017b) concluded that
 271 the interpreted magmatic foam substrate of the Ina mounds (abundant small
 272 vesicles with a bulk porosity up to ~95%) would result in superposed impact
 273 events characterized by energy partitioning that favored crushing of the void
 274 space below the projectile trajectory at the expense of lateral ejection. Thus
 275 crater diameters would be much smaller (~20-30% of the diameters of the same
 276 meteoritic impacts into typical mare regolith targets). Incorporating this
 277 "aerogel" effect of reduced impact crater diameter could readjust the observed
 278 crater retention age of less than 0.1 Ga to more than 3 Ga, coeval with the
 279 adjacent mare deposits. This ancient scenario complies with the conventional
 280 models of lunar geological and thermal evolutions, which predict that the
 281 continued net cooling of the Moon due to progressive heat loss by conduction
 282 caused mantle melting (magma source regions) to be deeper and much less
 283 abundant, and the global state of stress in the lithosphere to be increasingly
 284 contractional with time (Solomon & Head 1980; Head & Wilson 1992, 2017;
 285 Shearer et al. 2006; Ziethe et al. 2009). These factors combined to gradually
 286 inhibit the generation, ascent, and eruption of basaltic magma on the Moon,
 287 causing mare volcanic activity to diminish in middle lunar history

288 (Eratosthenian Period) and eventually to cease in the last ~1 Ga (Copernican
289 Period) (Hiesinger et al. 2011; Morota et al. 2011).

290 The geologically very recent small volcanic eruption origin scenario
291 (Braden et al. 2014), however, raises a line of questions that conflicts with
292 the above lunar evolution model, and indeed requires the overall evolution
293 history to be very different: (1) the current lunar interior would need to be
294 much hotter than previously thought, thus being able to maintain considerable
295 amounts of material near the melting point, (2) the abundance of heat-
296 producing elements (mainly Th, U, and K) in the lunar interior would have to
297 be much higher than prior estimations, and (3) at least parts of the lunar
298 lithosphere might be currently extensional in net state of stress, thus
299 assisting magma in the deep lunar interior in its ascent to the surface to
300 erupt. In addition, the IMPs are widely spread across the nearside maria and
301 half of them are outside the Procellarum KREEP Terrane (PKT), implying that
302 significant heat sources in many portions of the lunar interior persist to
303 geologically very recent time in order to account for the abundant small-
304 volume IMP eruptions. A major re-assessment of the current models of lunar
305 thermal evolution would be required if the very young volcanic eruption origin
306 for Ina/IMPs is verified.

307

308 **3. Synthesis of Predictions of the Two End-Member (Young and Old)** 309 **Models**

310 Current debate on the age and origin of Ina/IMPs centers on these two
311 competing theories: (1) geologically very young (late Copernican) small-volume
312 volcanic activity (Braden et al. 2014), and (2) ancient (Imbrian) volcanic
313 eruption producing highly vesicular magmatic foams (Qiao et al. 2017, 2018,
314 2019, 2020a, 2020b; Wilson & Head 2017b).

315

316 **3.1. The Young Model**

317 In the late Copernican volcanism scenario (Figure 3), the uneven/hummocky
318 floor terrains are solidified lava lake crust within the shield summit vent
319 being disrupted by lava drainage and deflation, and the smooth mounds are
320 subsequent small lobate lava flows extruded through the cracked floor crusts
321 (Braden 2013; Braden et al. 2014). The mounds within Ina are 2-20 m thick
322 (relative to the floor terrains), with an average value of 8 m, overlapping
323 with the thickness range of mare basalt flows (e.g., Schaber 1973; Hiesinger
324 et al. 2002). The convex-upward Ina mounds exhibit steep marginal scarps, with
325 an average margin slope of 26° (14-39°, 6-m-baseline), another piece of
326 evidence supporting a very young age for the Ina deposits.

327 Among the questions raised about the young volcanism interpretation are
328 the following:

329 (1) Continued net cooling of the Moon since middle lunar history would
330 have decreased average mantle temperature gradually, causing mantle melting to
331 be less abundant and magma source regions to be deeper. On the basis of
332 terrestrial analog observations (Hardee 1980), theory, and conductive cooling
333 calculations (e.g., Wilson & Head 1981; 2017a), the lava pond in the Ina IMP
334 could not have remained molten, following the last eruption, for more than a
335 few hundred to a thousand years, and thus is not a source for eruptions
336 occurring more than 3 billion years later. Bruce & Huppert (1989), Gonnermann
337 & Taisne (2015), and Wilson & Head (1981; 1988; 2017a) also show that any
338 magma in the dike connecting the source region to the surface would cool and
339 solidify even more rapidly. It is also highly unlikely that the magma source
340 region for the Ina shield volcano (at several hundred km depth) could remain
341 molten for the 3.4 Ga long interval between the Ina shield-building eruption
342 and any geologically very recent small magma extrusions within the 2 × 3 km
343 summit vent; such individual source regions are typically not active for times
344 in excess of tens to hundreds of millions of years (e.g., Wieczorek et al.
345 2006; Shearer et al. 2006; Marsh, 2015; Wilson & Head 2017a).

346 In addition, in order to extrude magma onto the surface from a molten
347 source region located at the great depth thought to be typical of the last
348 several hundred million years (Wieczorek et al. 2006; Shearer et al. 2006), a
349 higher excess pressure of basaltic diapirs (hence, greater magma source
350 volume) is required to reach the surface from such a deeper magma source
351 region. It seems highly implausible that magma would erupt from such a great
352 depth, and then be erupted in such small amounts (e.g., Wilson & Head 2017a;
353 Head & Wilson 2017).

354 (2) The shield volcano underlying the Ina summit pit crater is apparently
355 very ancient (e.g., Garry et al. 2012), dated to be ~3.5 Ga through crater
356 population analysis (Qiao et al. 2017, 2019), and thus formed during the major
357 global lunar mare volcanism phase ~3.3–3.8 Ga ago (Hiesinger et al. 2011).
358 Conventional models of lunar thermal evolution predict that, after ~3.5–3.6 Ga
359 ago, cooling of the outer portion of the Moon produced increasingly
360 compressive stress in the lunar lithosphere (Solomon & Head 1980). Could magma
361 rise from significant depths in recent thermal history of the Moon (in the
362 last several hundred million years) along pre-existing fractures (induced by
363 large impacts or rising diapirs)? Given the increasing overburden pressure
364 with depth and the thicker recent lithosphere (e.g., Wieczorek et al. 2006),
365 the closure of faults and cracks occurs at relatively shallow depths (Head &
366 Wilson 2020b) and it is thus highly unlikely that pre-existing fractures would
367 have remained open as pathways for rising magma for over 3 Ga. For these
368 reasons, the required dike propagation to the surface for volcanic eruptions
369 would be progressively more difficult with time in the period following the
370 initial Ina shield-building eruption. These factors suggest that it is
371 improbable that volcanic activity at the small Ina site would recur very

372 recently after having being dormant for ~3.4 Ga, with no evidence of at least
373 discontinuous activity during this long period.

374 (3) Imaging spectroscopic analysis show that both the raised mounds and
375 floor units within Ina have high-Ca pyroxene-dominated mineral composition
376 similar to that of the adjacent mare deposits (Bennett et al. 2015). This is
377 surprising, in that the young volcanism model thus predicts that the magma
378 reservoir or source region underwent no fractional crystallization or
379 contamination by fresh magmas in the ~3.4 Ga interval. **Although Bennett et al.**
380 **(2015) state that "a possible solution is that both the mare and Ina were**
381 **sourced from the deep mantle, which likely would not change its composition**
382 **greatly, even over such a long period of time", it seems much more likely, on**
383 **the basis of the mineralogical diversity of mare basalts in individual**
384 **locations with geologic time (e.g., Hiesinger et al. 2011), that the**
385 **composition would not remain the same.** Thus, it seems more plausible that the
386 multiple geological units within Ina were emplaced contemporaneously with the
387 background mare deposits ~3.5 Ga ago.

388 (4) The raised smooth mounds of Ina are among the most unusual terrains on
389 the lunar surface, with a range of morphological peculiarities, including
390 convex upward bulbous-like shapes, and marginal scarps and moats. Some young
391 Eratosthenian lava flows in southwestern Imbrium are also observed to exhibit
392 marginal scarps, but topographical moats are not observed at their flow
393 margins (Schaber 1973). If these Ina mounds are normal lava flows, why is
394 their morphology so different from that of other mare basalts? **For example,**
395 **the meniscus-like morphology (irregular, bleb-like shape with steep marginal**
396 **slopes) is unlike any morphology identified on the Moon in typical basaltic**
397 **landforms and deposits emplaced with basaltic lava rheology (Head & Wilson**
398 **2017).**

399 (5) Diviner thermophysical mapping results for Ina indicate that the Ina
400 interior is mantled by a surface regolith layer of measurable thickness (>10-
401 15 cm; Elder et al. 2017). **Synthesizing other thermophysical measurements**
402 **including thermal inertia, Elder et al. (2017) propose some process such as**
403 **explosive outgassing or pyroclastic eruptions as the origin of Ina and other**
404 **lunar IMPs.** Accumulation of a regolith layer of such thickness on geologically
405 very young lava flows (~33 Ma) seems unlikely, and would require an unusually
406 rapid development rate of lunar surface regolith (estimated to be 0.85 mm Ma⁻¹
407 over the last billion years by Quaide & Oberbeck 1975; a 33 Ma-old lava flow
408 would accumulate a layer of regolith materials only ~2.8 cm thick).

409 (6) **Basilevsky & Michael (2020, 2021) show that the morphology of young**
410 **craters superposed on the Ina mounds is identical to that of craters on**
411 **typical ancient mare surfaces, and interpret this to disproves the hypothesis**
412 **that the mounds are formed of magmatic foams, and that this supports the**
413 **relatively recent origin of the mounds. However, it has been documented**
414 **(Zanetti et al. 2017; Plescia & Robinson 2019), that craters superposed on**

415 tens of millions of years old impact melt deposits (fresh solidified bedrock)
416 in large young craters have very different morphology from those in mature
417 regolith. Thus, if the mounds were indeed young effusive basaltic volcanic
418 features, we would expect small crater morphologies to be similar to those in
419 young impact melts. Thus, the arguments of Basilevsky & Michael (2020, 2021)
420 could be cited to support an ancient age for the mound material.

421

422

3.2. The Old Model

423

424 The Imbrian-age volcanic eruption model provides an alternative
425 interpretation for the age and origin of Ina and IMPs. In this scenario, the
426 formation of various morphological units within Ina are basically the natural
427 consequences of the latest stage of dike emplacement and magma degassing in
428 the summit crater atop a small lunar shield volcano ~3.5 Ga ago (Figure 4).
429 Specifically, the floor hummocky units are interpreted as a chilled lava pond
430 crust and the raised mounds as final-phase small magma extrusions (Qiao et al.
431 2017, 2018, 2019, 2020a, 2020b; Wilson & Head 2017b). In addition, waning-
432 stage summit pit/vent activities under the unique lunar conditions of low
433 gravitational acceleration and essentially zero-atmospheric pressure produce
434 unusually vesicular eruption deposits neither predicted nor observed on
435 terrestrial final-stage eruptions. Extremely porous macro-vesicular lava lake
436 floor deposits are interpreted to favor drainage of subsequently produced
437 regolith into the substrate and enhance the retention of optical immaturity
438 and blockiness. Mounds are interpreted as the viscous extrusions of foamy
439 magma that had collected below the lava lake floor in the terminal stages of
440 the eruption. The highly vesicular substrate property of the extruded mounds
441 is interpreted to exert notable effects on the post-emplacement impact
442 cratering process (energy partitioning) and produced anomalously young crater
443 retention ages (<0.1 Ga).

443

444 Difficulties and critical unresolved issues also characterize the ancient,
445 shield-contemporaneous summit lava lake magmatic foam eruption interpretation
446 for Ina.

446

447 (1) How to convincingly explain the deficit of superposed impact craters
448 and the resulting extremely young CSFD model ages of Ina interior deposits?
449 Although the predicted unusually porous substrate characteristics of the Ina
450 mounds and the consequent crater size decrease effect have been called on to
451 account for the young crater counting ages of the Ina interior (Qiao et al.
452 2017, 2019; Wilson & Head 2017b), it should be noted that the consequences of
453 impact cratering into highly porous materials and its effect on crater sizes
454 are not yet fully understood, due to many difficulties in both laboratory
455 impact experiments and numerical simulations. Additional dedicated
456 theoretical, experimental and numerical studies of impact cratering into
porous substrates should help to clarify the age debate on Ina and lunar IMPs,

457 and would also enhance our knowledge of surface processes on many porous
458 asteroid bodies.

459 (2) Meteoritic impacts into the Ina foamy mounds were predicted to produce
460 smaller and deeper ("cylinder-like" or "hole-like"), and non-blocky craters
461 (Wilson & Head 2017b; Qiao et al. 2017). However, no such unusual craters are
462 apparently seen on the Ina mounds (Basilevsky & Michael 2020, **2021**). Instead,
463 many impact craters superposed on the smooth mounds exhibit a range of
464 characteristics of typical impact craters developed on mare regolith,
465 including raised rims, ejecta deposits, blocky interiors, a range of
466 degradations, and smaller depth-to-diameter ratios (Wagner et al. 2018;
467 Basilevsky & Michael 2020, **2021**). This appears to contradict the foam origin
468 model for the Ina mounds. Additional work on the nature of "auto-regolith"
469 development on extruded foamy lavas (e.g., Wilson & Head 2017b) needs to be
470 undertaken, as well as on the nature of basaltic volcanic protoliths in
471 general (e.g., Head & Wilson **2020a**).

472 (3) The Ina floor terrains, especially the floor rubble materials, are
473 characterized by unusually high reflectance and optical immaturity (Schultz et
474 al. 2006; Garry et al. 2013; Bennett et al. 2015; Qiao et al. 2019). Any
475 materials exposed to the harsh space environment of the lunar surface,
476 including micrometeorite bombardment, cosmic and solar ray irradiation, and
477 solar wind implantation, are equally subject to space weathering modification
478 process (Pieters & Noble 2016). Over a >3 Ga period of space weathering
479 processes, significant modification of the optical properties of the Ina floor
480 materials should occur, resulting in surface darkening and optical maturation,
481 possibly resembling that of the mare regolith surface surrounding the Ina pit
482 crater. Although the conceptual model of regolith drainage into the predicted
483 macro-vesicular void space of the lava lake floor may be plausible, a
484 quantitative model to account for this process, the filling of the void space,
485 the drainage-inducing processes, and the associated effects on optical
486 maturation, has not yet been formulated. Thus, it is unknown whether the
487 model-predicted porous substrates have significant effects on space weathering
488 processes on the lunar surface and, if so, how these effects map out into
489 specific observed optical alteration properties.

490 (4) The contacts between Ina mounds and floor terrains are typically
491 characterized by very steep scarps and adjacent moats, some of which have the
492 steepest topographic slopes ($\sim 32^\circ$) on the Moon (Qiao et al. 2019), leading
493 Fassett and Thompson (2015) to propose that these troughs must have been
494 formed within the last 1-2 Ma, or perhaps are still currently forming. Any
495 ancient model of Ina origin must also explain how to maintain the very sharp
496 contacts at Ina over 3.5 billion years in a progressive topographic erosion
497 environment predominantly induced by a steady impact crater flux, which serves
498 to topographically smooth and mute such distinctive surface relief over time
499 (Fassett & Thompson 2014). Although the moats have been attributed to

500 subsurface foam evacuation, loading, flexure, and regolith drainage (e.g.,
501 Wilson & Head 2017b), it is still intuitively unclear how these processes
502 could result in such sharp and distinctive moats and contacts.

503

504

3.3. Summary

505 We thus conclude that in order to resolve the differences between these
506 two hypotheses for the origin of Ina, new data, experiments, and missions are
507 required. In the following sections we first identify the key **observations and**
508 measurements that would help distinguish between the two models, and then
509 define a range of mission types that could be undertaken to provide these
510 data. For simplicity, we refer to the Braden et al. (2014) hypothesis (Figure
511 3) as the Ina-is-younger model (**Young-model**), and the Qiao et al. (2017, 2019)
512 shield-contemporaneous ~3.5 Ga model as the Ina-is-older model (**Old-model**).

513

514 4. Key Observations and Measurements to Distinguish between the End- 515 member Models

516 In this section, we list a sequence of key observations and measurements
517 from the Ina surface and on samples that would help explain the range of
518 enigmatic features in Ina and resolve key questions concerning the origin of
519 Ina, especially the "age question": What is the age of the units comprising
520 the Ina IMP (mounds and floor unit)? Concurrent with the emplacement of the
521 small shield volcano and surrounding mare deposits, and thus over three
522 billion years old? Formed in the last few tens of millions of years, as
523 interpreted from superposed impact crater size-frequency distributions?; and
524 the "mode of origin of the units question": What is the origin of the units
525 comprising the Ina IMP (mounds and floor unit)? Minor variations on typical
526 lunar mare basalt lava flow emplacement processes? Major variations in the
527 vesicularity and physical properties of basaltic magmas intruded in the
528 terminal phases of shield volcano summit pit crater eruptions? In particular,
529 these observations and measurements would help distinguish between the two
530 end-member models: Young-model (Braden et al. 2014) and Old-model (Qiao et al.
531 2017, 2019).

532 (1) Radiometric ages of the Ina mounds and floor materials: Acquisition
533 and radiometric dating of samples of the material that makes up the mounds and
534 floor units would provide unequivocal evidence to distinguish between the two
535 models. **These measurements are necessary and sufficient to unambiguously**
536 **resolve the key question concerning the formation age of Ina deposits.** The
537 magnitude of the age difference between the two models (>3.4 Ga or a factor of
538 over 100) is so large that perhaps even in-situ age determination (e.g.,
539 Anderson et al. 2017) could resolve the controversy.

540 (2) Characteristics of the regolith material on the mounds and on the
541 floor: Predictions of the **Young-model** suggest that the regolith is derived

542 from recently emplaced basalts and thus the regolith development from this
543 protolith (Head & Wilson 2020a) should be standard impact fragmentation of
544 solid basalt to produce a regolith. The **Old-model**, on the other hand, predicts
545 that the mound protolith will be very vesicular magmatic foam, with an
546 "autoregolith" of explosively fragmented bubble wall shards and an impact-
547 induced regolith produced from, and on top of, this substrate. The floor unit
548 is predicted to be composed of macro-vesicular basalt with regolith draining
549 into the void spaces, leaving larger and optically immature particles and
550 rocks on the surface. Thus, there should be a clear distinction possible
551 between the two models on the basis of the predicted substrate
552 characteristics. In-situ observations (high-resolution images of regolith
553 particles in both terrains to assess their grain size, shape, optical
554 maturity, agglutinates, proportion of glass, etc.), sieves to assess particle
555 size distributions, and observations to assess the nature of the moats and
556 search for evidence of macro-vesicular voids and associated regolith drainage
557 in the floor units and subunits. **In addition, detailed Ina regolith property**
558 **analyses would also help test or verify other formation theories of Ina (Table**
559 **1). For instance, if typical normal mare regolith characteristic is observed,**
560 **it is also consistent with the recent gas released-induced removal of ancient**
561 **regolith model (Schultz et al. 2006).**

562 (3) 3-D structure of the mounds and floor material (porosity): Emplacing
563 core tubes in the upper meters of the floor and mound regolith deposits would
564 be a significant step in documenting the vertical structure, variability and
565 origin of the regolith. A much more comprehensive view could be obtained by
566 ground penetrating radar (GPR) surveying (e.g., Xiao et al. 2015; Lai et al.
567 2019; Li et al. 2020) of the mound and floor units. Seismic profiling could
568 also determine the nature of the mound and floor unit three-dimensional
569 structure, and readily distinguish between the normal basaltic substrate of
570 the **Young-model** and the highly macro- and micro-vesicular nature of the **Old-**
571 **model**.

572 (4) Regolith thickness; any change with depth on mound and floor material:
573 Comparison of regolith thickness (and nature) through coring, GPR and seismic
574 studies will also be critical in distinguishing between the **Old-model** (thicker
575 and more mature regolith developed over >3.4 Ga) and **Young-model** (much thinner
576 and patchy regolith developed over ~33 Ma).

577 (5) Nature of ejecta from craters into mound and floor material:
578 Assessment of the morphology and frequency distribution of superposed impact
579 craters of different sizes will help in identifying any distribution that
580 might deviate from standard basaltic morphologies and proportions, or
581 alternatively that might signal the presence of a substrate or regolith of
582 foamy or marco-vesicular nature. Analysis and sampling of crater ejecta from
583 different sized craters will also reveal changes in the substrate with depth
584 that will distinguish between the **Old- and Young-model** predictions.

585 (6) Level of vesicularity of surface rocks: Surface observations and
586 analysis of crater ejecta indicating subsurface layers, and their level of
587 vesicularity will also help to distinguish between the two hypotheses, with
588 **Old-model** predictions requiring very significant macro-vesicularity in the
589 floor units, and magmatic foam-level vesicularity in the mound unit.

590 (7) Volatile content of magma petrogenesis: Return of samples to Earth for
591 laboratory analysis and petrogenetic probing will provide essential data to
592 identify depth of origin of magmas, petrogenetic pathways, and the nature and
593 amount of volatiles necessary to produce magmatic foams.

594 (8) Comparison of rocks, soils (and ages) inside Ina and on the shield
595 rim: An extended traverse to the Ina shield volcano rim and flanks, the
596 collection of samples there to compare with those collected on the floor of
597 Ina, and analysis of comparative ages, vesicularities and petrogenesis would
598 provide conclusive evidence to distinguish between the **Old- and Young- models**
599 for the origin of Ina.

600 (9) Paleomagnetism measurements: In-situ magnetic analyses, or laboratory
601 analysis of returned samples, would provide important evidence to distinguish
602 between the two hypotheses. Magnetized samples would support the **Old-**
603 **hypothesis** as the lunar magnetic field is interpreted to have been active at
604 ~3.5 Ga, but to have decayed by the time (~33 Ma) derived from CSFD ages
605 (Weiss & Tikoo 2014).

606

607 5. Missions Capable of Addressing these Objectives

608 In this section we present an assessment of several mission styles and
609 modes, optimal landing sites, and where appropriate, conceptual traverses. We
610 conclude with a human landing and exploration design reference mission (DRM).

611 (1) Robotic lander Mission (with or without hopping mobility): A single
612 robotic lander mission with no mobility (e.g., Stopar et al. 2019) could
613 significantly contribute to distinguishing between the two hypotheses by
614 carrying a payload consisting of a high-resolution multispectral imager, a
615 microscopic imager for grain size and morphology, a magnetometer, a scoop to
616 dig into the subsurface and assess the mechanical properties of the regolith,
617 an in-situ GPR as manifested on the Chang'e-5 lunar lander (Li et al. 2019b;
618 Xiao et al. 2019), and, if possible, an in-situ geochronology instrument to
619 clarify the age debate of Ina deposits (e.g., a K-Ar laser experiment
620 developed by Cohen et al. 2014). If limited to a single mission, the
621 spacecraft should land on a mound on the floor of Ina (e.g., Stopar et al.
622 2019 and Figure 5), as the mound characteristics (basaltic regolith versus
623 magmatic foam regolith and auto-regolith) are the most prominent predictions
624 to distinguish between the two models **and test other formation theories of Ina**
625 **(Table 1)**.

626 Hopping capability would significantly assist in assuring representative
627 measurements and determining diversity within the mound, and long hops or

628 multiple hops might permit access to the floor units as well. Multiple landing
629 missions would also accomplish these goals.

630 (2) Robotic Sample Return Mission: The most conclusive results to
631 distinguish between the models would result from a sample return mission. A
632 robotic probe, similar to the Chang'e-5 sample return mission profile (Li et
633 al. 2019a), to a mound landing site would be ideal (e.g., Figure 5), with
634 imaging systems to document the local setting, GPR to probe the subsurface
635 regolith and bedrock structure, a scoop to assess the upper parts of the
636 regolith and collect samples, and a meters-scale core to sample with depth.
637 Returned to Earth, these samples could be fully assessed from a geologic,
638 chronologic, geophysical, and petrogenetic perspective and a clear and concise
639 answer could be obtained.

640 (3) Robotic Rover Mission: Addition of mobility to a lander mission would
641 significantly enhance the science return and not only distinguish among the
642 hypotheses, but also help to understand the actual array of processes involved
643 in the formation of the Ina structure (and similar features such as Sosigenes,
644 Cauchy 5, and the population of smaller IMPs (Braden et al. 2014; Qiao et al.
645 2020a)). For example, rovers could traverse from a landing on the relatively
646 smoother mounds to the mound flanks, the various units on the Ina floor, and
647 perhaps even to the rim of the pit crater to compare and contrast the
648 characteristics of the Ina floor with those of the shield volcano itself
649 (Figure 6). Traverse geology (imaging and trafficability), geophysics
650 (magnetic, seismic, and GPR traverses), detailed sample analyses
651 (multispectral mineralogy and microscopic imaging), as well as the ability to
652 probe the upper meters of regolith (scoops and rover tracks) are also
653 essential.

654 (4) Human Landing and Exploration Mission: With a resurgence of interest
655 in lunar exploration, including China's continued Lunar Exploration Program
656 (CLEP), the NASA program of "Forward to the Moon with Artemis," and the
657 parallel and cooperative human exploration endeavors of ESA, Russia, India,
658 and others, human exploration of the Moon is clearly feasible in the first
659 half of the 21st century. Here we present a design reference mission for an
660 Apollo J-Mission-scale expedition to the Ina summit pit crater and vicinity
661 (Figure 7), designed specifically to resolve the issue of the two (old and
662 young) origins for the Ina crater interior, but more importantly to provide
663 the data to establish a refined or new model that can help explain these
664 enigmatic features in Ina, as well as other large features such as Sosigenes
665 and Cauchy 5, and the many dozens of smaller IMPs in the lunar maria (e.g.,
666 Braden et al. 2014; Qiao et al. 2020a).

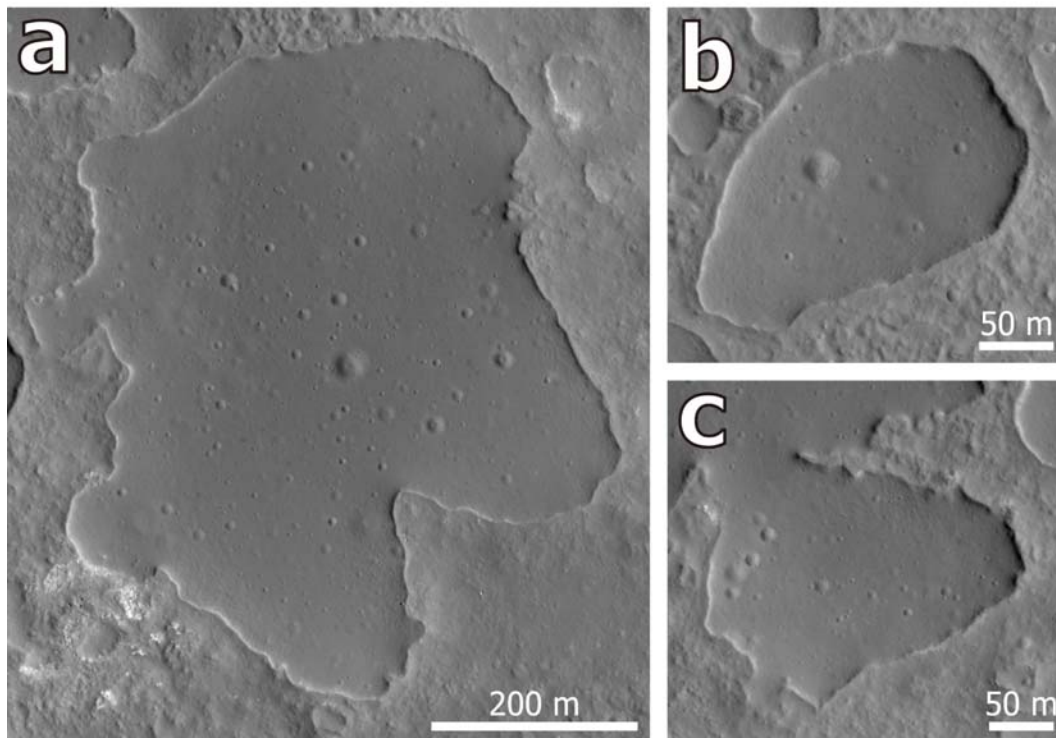
667 In this "Design Reference Mission" (Figure 7), we propose landing on the
668 floor of Ina on the largest of the mounds (formally named Mons Agnes, Figure
669 7) and deploying ALSEP (Apollo Lunar Surface Experiments Package)-like
670 geophysical monitoring stations, and undertaking extensive coring and analysis

671 of the regolith and substrate of the mounds, sampling laterally within walking
672 distance with meters-scale cores and extensive geologic observations and
673 sampling, guided by Astronaut visual observations and in-situ GPR data.
674 Following the first EVA (extravehicular activity; yellow path in Figure 7),
675 the crew would traverse due east, down the flanks of the mound, across the
676 moat (labelled in Figure 7), stopping to examine the characteristics and
677 morphology of the moat structure, before proceeding across the more mature
678 floor regolith deposits. Samples and observations here from traverse
679 geophysics and GPR data will help measure the substrate density and search for
680 evidence of macro-vesicularity predicted by the **Old-model**. The second traverse
681 (gold path in Figure 7) continues to the bright and optically immature blocky
682 unit and outcrops at the eastern margin of the Ina floor (labelled in Figure
683 7), where stratigraphy may also be exposed in the marginal scarp. Following
684 analysis of the floor margin contact, the traverse would continue up the wall
685 of the pit crater to the rim to continue traverse geophysics and sampling to
686 compare the ancient rim of the shield volcano with the potentially >3 Ga
687 younger floor (Figure 7). The traverse would then extend along the southeast
688 rim of the pit crater, obtaining perspective views and measurements of the Ina
689 interior, and then descend down to the pit crater floor at the "vermicular"
690 terrain, before heading to the western margin of the largest Ina mound and
691 moat, and ascending the mound back to the landing site (Figure 7). Total
692 traverse distance of the first EVA would be about 3.2 km, a modest distance
693 compared with Apollo J-Mission traverses. The second EVA (traverse 3 shown as
694 the blue path in Figure 7) would traverse from the landing site in a west-
695 southwest direction, crossing multiple mounds for comparison with the major
696 mound, its moat margins and the intervening floor subunits, and would have as
697 a target, an unusual blocky impact crater on the southwest Ina floor (Ivanov &
698 Head 2019, labelled in Figure 7). Here, exploration and analysis of the
699 unusual nature of impact craters and the stratigraphic relationships between
700 mounds and floor units will significantly assist in the determination of the
701 origin of the Ina floor deposits and the specific processes operating to form
702 them. A fourth traverse (cyan path in Figure 7) explores the northern and
703 northwestern part of the Ina floor, providing additional characterization of
704 the Ina floor units and their three-dimensional structure. The astronauts
705 would traverse down onto a peculiar "low" mound feature (labelled in Figure 7)
706 in the northern floor. This "low" mound is ~100x80 m in size, the largest one
707 among six "low" mounds identified in Ina interior floor with smooth surface
708 textures and lower elevations than the surrounding terrains (Qiao et al.
709 2019). These extensive geologic field investigations and sampling of Ina's
710 materials will provide fundamental insights into its characteristics and
711 formation mechanisms. Together, these four traverses cover a total distance of
712 about 11.6 km (Figure 7), well within the range for the successful Apollo J-
713 missions (~28-36 km in Apollo 15, 16, and 17). Clearly, human exploration and

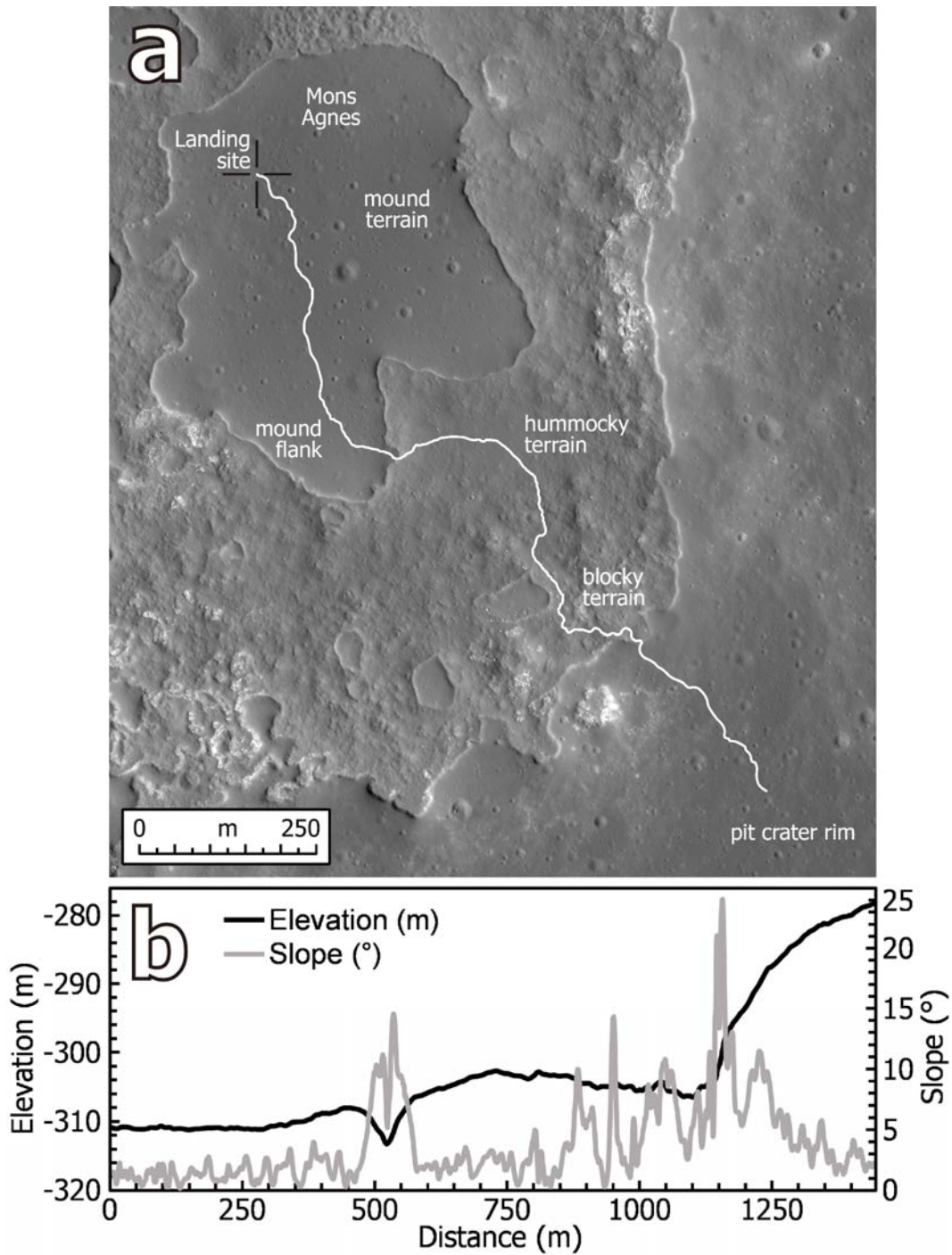
714 associated mobility provide significantly more scientific results than can be
715 obtained by a robotic mission alone.

716 However, the nature of slopes and the physical structure of regolith along
717 the proposed traverses (Figures 6 and 7) may present some challenges to human
718 and robotic exploration. For example, the slopes at the margins of mounds in
719 our traverse may sometimes exceed those encountered by Lunokhod and Apollo
720 rovers (Basilevsky et al. 2019) and thus engineering designs and operational
721 strategies need to take this into consideration. In addition, the macro-
722 porosity and regolith characteristics predicted by some models (e.g., magmatic
723 foam mounds and macro-porous floor; Qiao et al. 2017, 2019; Wilson & Head
724 2017b) may introduce potential trafficability and soil particle contamination
725 problems that should be taken into consideration during mission planning
726 (e.g., including ground penetrating radar instruments; design to accommodate
727 very fine angular particles).

728

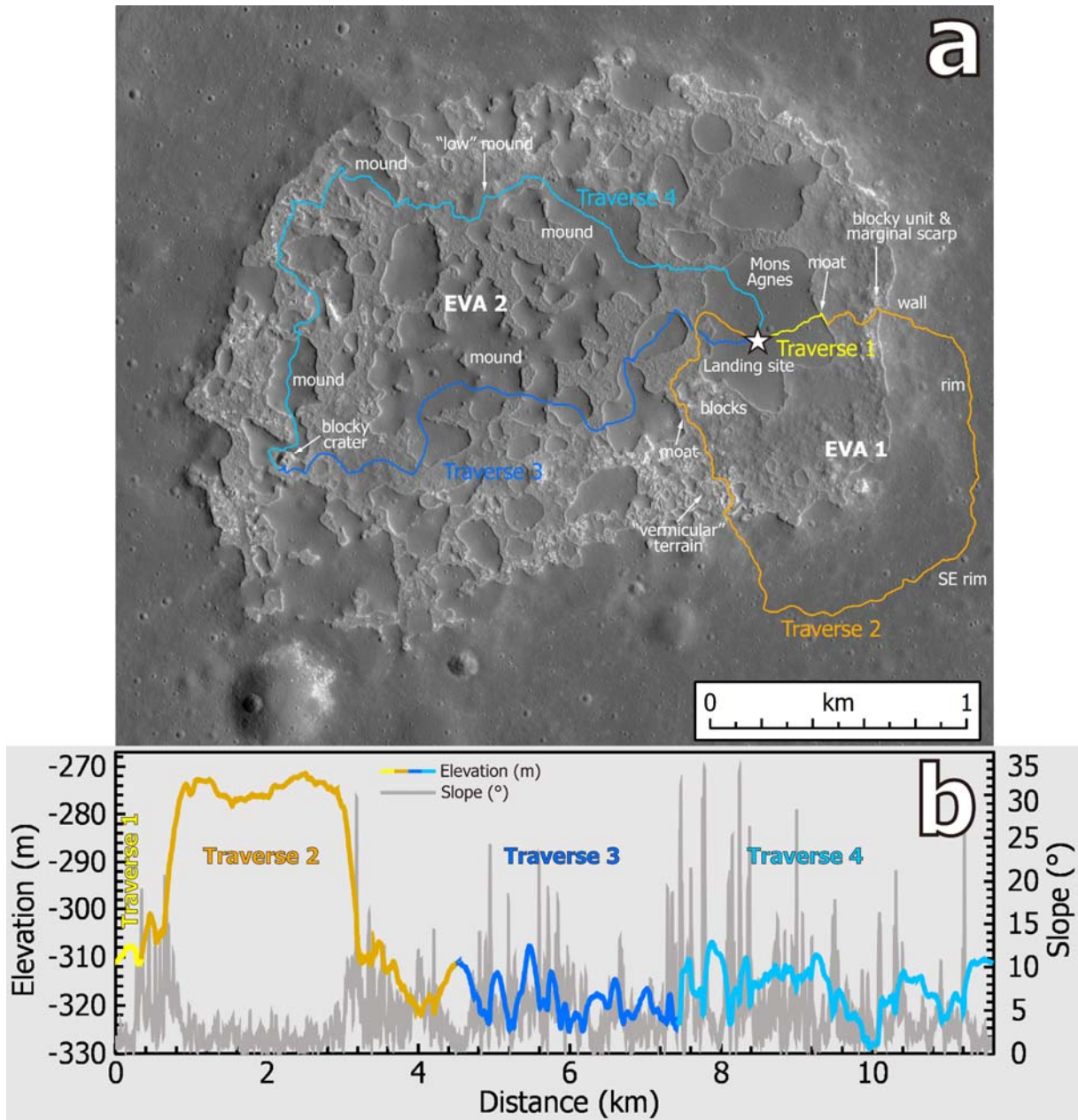


729 **Figure 5.** LROC NAC images of mound terrains (all cropped from frame
730 M119815703) proposed as landing targets for robotic lander and/or sample
731 return missions.
732
733



734
 735
 736
 737
 738
 739
 740

Figure 6. (a) Proposed landing site (marked by the black cross hair) and traverse path for a robotic rover mission to the Ina pit crater; surface investigation sites are labelled. The background is cropped from LROC NAC frame M119815703. (b) LROC NAC DTM elevation (black line) and slope (grey line) profiles along the traverse path.



741
 742 **Figure 7. (a)** Traverse map of our proposed human landing and exploration
 743 "Design Reference Mission" to the Ina pit crater and vicinity, showing the
 744 suggested landing site (star symbol) on the largest mound (Mons Agnes),
 745 astronaut traverse paths during the first (including traverse 1 and 2) and
 746 second (including traverse 3 and 4) extravehicular activities (EVA), and
 747 scientific investigations sites (labelled by terrain names). The background is
 748 cropped from LROC NAC frame M119815703. **(b)** LROC NAC DTM elevation (color
 749 line) and slope (grey line) profiles along the traverse paths.

750

751

6. Conclusions

752 The Ina pit crater is one of the most mysterious lunar features identified
753 and investigated during the Apollo era (Whitaker 1972; El-Baz 1973). Its range
754 of geological peculiarities has perplexed lunar scientists for decades and
755 resulted in a wide variety of hypotheses for their origins. Ina is also the
756 most notable representative of a group of dozens of small mare features,
757 identified on high-resolution LROC NAC images and termed Irregular Mare
758 Patches (IMPs; Stooke 2012; Braden et al. 2014). However, the specific
759 formation mechanism and emplacement age of Ina and other lunar IMPs have been
760 long debated, and various competing theories have been proposed to account for
761 the characteristics, age, and origin of Ina/IMPs (Table 1). One of the most
762 contentious issues concerning Ina's origin is the actual emplacement age,
763 especially the disparity between the geologically very young (<0.1 Ga) small
764 volcanic eruption model (**Young-model**; Braden et al. 2014) and the very old (>3
765 Ga) magmatic foam extrusion hypothesis (**Old-model**; Qiao et al. 2017, 2018,
766 2019, 2020a, 2020b; Wilson & Head 2017b). Distinguishing between the two
767 competing theories will provide vital constraints on the cessation time of
768 lunar mare volcanism, either the previously established ~1 Ga ago (Hiesinger
769 et al. 2011; Morota et al. 2011) or the recently proposed geologically very
770 recent ~18 Ma (Braden et al. 2014); this is a key parameter for modeling the
771 geological and thermal evolution of the Moon.

772 We conclude that in order to resolve the controversy between these two
773 very different scenarios for the origin and age of Ina, new data, experiments,
774 and sample returns from new landed lunar missions are required. **To**
775 **unequivocally resolve the question of the ancient or recent age of the Ina**
776 **irregular mare patch, a robotic sample return mission, such as the recent**
777 **Chang'e-5 mission (Li et al. 2019a), is required. In order to unequivocally**
778 **resolve the question of the origin of the geologic units comprising the Ina**
779 **IMP, a robotic rover or human exploration mission that can traverse and**
780 **examine the soils, rocks and substructure of the units is required.** In this
781 contribution, we identify key measurements from the Ina surface and on samples
782 that would help distinguish between the two end-member models, including
783 radiometric ages of Ina deposits, the nature of regolith materials, 3-D
784 shallow subsurface structure, volatiles involved in magma petrogenesis, and
785 paleomagnetism. In the current international circumstances of a resurgence of
786 lunar exploration endeavors, we define a range of conceptual lunar missions to
787 the Ina feature, including mission styles, optimal landing sites, and
788 conceptual traverses for robotic lander and/or rover missions, robotic sample
789 return missions, and human landings and exploration. These missions will
790 provide vital data not only to resolve the issue of the two (old and young)
791 origins for the Ina crater interior, but also more importantly to establish a
792 refined or new model that can help explain these enigmatic features in Ina, as
793 well as other large features such as Sosigenes and Cauchy 5, and the many

794 dozens of smaller IMPs in the lunar maria (e.g., Braden et al, 2014; Qiao et
795 al., 2020a).

796

797

Acknowledgments

798

799

800

801

802

803

804

805

806

References

807

808

809

810

811

812

813

814

815

816

817

818

819

820

821

822

823

824

825

826

827

828

829

830

831

832

833

834

835

836

This study is supported in part by the National Key R&D Program of China (No. 2020YFE0202100), Pre-research Projects on Civil Aerospace Technologies Nos. D020205 and D020102 funded by CNSA, and the National Natural Science Foundation of China (No. 41703063, 11941001, and 41972322). J. W. H. gratefully acknowledges financial support from the NASA Lunar Reconnaissance Orbiter Lunar Orbiter Laser Altimeter (LOLA) experiment (grants NNX09AM54G and NNX11AK29G) at Brown University.

- Anderson, F. S., Whitaker, T. J., Wiesendanger, R., Wurz, P., Beck, S., & Levine, J. 2017, 5th European Lunar Symposium (Münster, Germany: University of Münster), 25
- Basilevsky, A. T., et al. 2019, Solar System Research, 53, 383**
- Basilevsky A. T. & Michael G. G. 2020, 11th Moscow Solar System Symposium (Moscow, Russia: Space Research Institute), 209
- Basilevsky A. T. & Michael G. G. 2021, Solar System Research, 55, 20**
- Bennett, K. A., Horgan, B. H. N., Bell, J. F., III, Meyer, H. M., & Robinson, M. S. 2015, 46th Lunar and Planetary Science Conference (The Woodlands, Texas: Lunar and Planetary Institute), abstract #2646.
- Braden, S. E. 2013, Analysis of spacecraft data for the study of diverse lunar volcanism and regolith maturation rates (Tempe, Arizona: Arizona State University)
- Braden, S. E., Stopar, J. D., Robinson, M. S., Lawrence, S. J., van der Bogert, C. H., & Hiesinger, H. 2014, Nat Geosci, 7, 787
- Bruce, P. M., & Huppert, H. E. 1989, Nature, 342, 665**
- Carter, L. M., Hawke, B. R., Garry, W. B., Campbell, B. A., Giguere, T. A., & Bussey, D. B. J. 2013, 44th Lunar and Planetary Science Conference (The Woodlands, Texas: Lunar and Planetary Institute), abstract #2146.
- Cernan, E. A., Evans, R. E. & Schmitt, H. 1972, Apollo 17 technical air-to-ground voice transcription (Houston, Texas: Manned Spacecraft Center)
- Cohen, B. A., Miller, J. S., Li, Z.-H., Swindle, T. D., & French, R. A. 2014, Geostandards and Geoanalytical Research, 38, 421
- Defense Mapping Agency 1974, National Aeronautics and Space Administration Lunar Topophotomap 41C3S1(10) (Washington, DC: Defense Mapping Agency Topographic Center)
- El-Baz, F. 1972. 3rd Lunar and Planetary Science, ed. E. A. King, D. Heymann, & D. R. Criswell (Houston, Texas: Lunar and Planetary Institute), 39
- El-Baz, F. 1973, in Apollo 17 Preliminary Science Report (Washington, DC: United States Government Printing Office), 30-13

837 Elder, C. M., Hayne, P. O., Bandfield, J. L., Ghent, R. R., Williams, J. P.,
838 Donaldson Hanna, K. L., & Paige, D. A. 2017, *Icarus*, 290, 224
839 Evans, R. E., & El-Baz, F. 1973, in Apollo 17 Preliminary Science Report
840 (Washington, DC: United States Government Printing Office), 28-1
841 Fassett, C. I., & Thomson, B. J. 2014, *J Geophys Res-Planet*, 119, 2255
842 Fassett, C. I., & Thomson, B. J. 2015, 46th Lunar and Planetary Science
843 Conference (The Woodlands, Texas: Lunar and Planetary Institute), abstract
844 #1120.
845 Garry, W., et al. 2012, *Journal of Geophysical Research*, 117, E00H31
846 Garry, W. B., Hawke, B. R., Crites, S., Giguere, T., & Lucey, P. G. 2013, 44th
847 Lunar and Planetary Science Conference (The Woodlands, Texas: Lunar and
848 Planetary Institute), abstract #3058.
849 **Gonnermann, H., & Taisne, B. 2015, in *The Encyclopedia of Volcanoes (Second***
850 ***Edition)*, ed. H. Sigurdsson (Amsterdam: Academic Press), 215**
851 **Hardee, H. C. 1980, *Journal of Volcanology and Geothermal Research*, 7, 211**
852 Head, J., & Gifford, A. 1980, *The Moon and the Planets*, 22, 235
853 Head, J. W., & Wilson, L. 1992, *Geochim Cosmochim Acta*, 56, 2155
854 Head, J. W., & Wilson, L. 2017, *Icarus*, 283, 176
855 Head, J. W., & Wilson, L. 2020a, *Geophys Res Lett*, 47, e2020GL088334
856 **Head, J. W., & Wilson, L. 2020b, *Planet Space Sci*, 180, 104765**
857 Hiesinger, H., Head III, J., Wolf, U., Jaumann, R., & Neukum, G. 2002, *Geophys*
858 *Res Lett*, 29, 1248
859 Hiesinger, H., Head, J. W., Wolf, U., Jaumann, R., & Neukum, G. 2011,
860 *Geological Society of America Special Papers*, 477, 1
861 Ivanov, B. A., & Head, J. W. 2019, 50th Lunar and Planetary Science Conference
862 (The Woodlands, Texas: Lunar and Planetary Institute), abstract #1243
863 Lai, J., et al. 2019, *Geophys Res Lett*, 46, 12783
864 Li, C., et al. 2020, *Science Advances*, 6, eaay6898
865 Li, C., Wang, C., Wei, Y., & Lin, Y. 2019a, *Science*, 365, 238
866 Li, Y., Lu, W., Fang, G., Zhou, B., & Shen, S. 2019b, *Advances in Space*
867 *Research*, 63, 2267
868 **Marsh, B. D. 2015, in *The Encyclopedia of Volcanoes (Second Edition)*, ed. H.**
869 ***Sigurdsson (Amsterdam: Academic Press), 185***
870 Morota, T., et al. 2011, *Earth Planet Sc Lett*, 302, 255
871 **Plescia, J. B., & Robinson, M. S. 2019, *Icarus*, 321, 974**
872 Pieters, C. M., & Noble, S. K. 2016, *Journal of Geophysical Research: Planets*,
873 121, 1865
874 Qiao, L., Head, J., Wilson, L., Xiao, L., Kreslavsky, M., & Dufek, J. 2017,
875 *Geology*, 45, 455
876 Qiao, L., Head, J. W., Xiao, L., Wilson, L., & Dufek, J. D. 2018, *Meteorit*
877 *Planet Sci*, 53, 778
878 Qiao, L., Head, J. W., Ling, Z., Wilson, L., Xiao, L., Dufek, J. D., & Yan, J.
879 2019, *Journal of Geophysical Research: Planets*, 124, 1100

880 Qiao, L., Head, J. W., Ling, Z., & Wilson, L. 2020a, *Journal of Geophysical*
881 *Research: Planets*, 125, e2019JE006362
882 Qiao, L., Head, J. W., Wilson, L., & Ling, Z. 2020b, *Journal of Geophysical*
883 *Research: Planets*, 125, e2019JE006171
884 Quaide, W., & Oberbeck, V. 1975, *The Moon*, 13, 27
885 Robinson, M. S., et al. 2010, *Space Sci Rev*, 150, 81
886 Schaber, G. G. 1973, 4th Lunar and Planetary Science (Houston, Texas: Lunar
887 and Planetary Institute), 73
888 Schultz, P. H., Staid, M. I., & Pieters, C. M. 2006, *Nature*, 444, 184
889 Shearer, C. K., et al. 2006, *Reviews in Mineralogy and Geochemistry*, 60, 365
890 Solomon, S. C., & Head, J. W. 1980, *Reviews of Geophysics*, 18, 107
891 Stooke, P. J. 2012, 43rd Lunar and Planetary Science Conference (The
892 Woodlands, Texas: Lunar and Planetary Institute), abstract #1011
893 Stopar, J. D., et al. 2019, *Planet Space Sci*, 171, 1
894 Strain, P. L., & El-Baz, F. 1980. 11th Lunar and Planetary Science Conference
895 (Houston, Texas: Lunar and Planetary Institute), 2437
896 Wagner, R., Denevi, B. W., Stopar, J. D., van der Bogert, C. H. & Robinson, M.
897 S. 2018. Lunar Science Targets for Landed Missions (Moffett Field,
898 California: NASA Ames Research Center), abstract #LLW2018-15.
899 Weiss, B. P., & Tikoo, S. M. 2014, *Science*, 346, 1246753
900 Whitaker, E. A. 1972, in *Apollo 15 Preliminary Science Report* (Washington, DC:
901 United States Government Printing Office), 25-84
902 **Wieczorek, M. A., et al. 2006, *Reviews in Mineralogy and Geochemistry*, 60, 221**
903 **Wilson, L., & Head III, J. W. 1981, *Journal of Geophysical Research: Solid***
904 ***Earth*, 86, 2971**
905 **Wilson, L., & Head III, J. W. 1988, *Journal of Geophysical Research: Solid***
906 ***Earth*, 93, 14785**
907 Wilson, L., & Head, J. W. 2017a, *Icarus*, 283, 146
908 Wilson, L., & Head, J. W. 2017b, *Journal of Volcanology and Geothermal*
909 *Research*, 335, 113
910 Wilson, L., & Head, J. W. 2018, *Geophys Res Lett*, 45, 5852
911 Xiao, L., et al. 2015, *Science*, 347, 1226
912 Xiao, Y., Su, Y., Dai, S., Feng, J., Xing, S., Ding, C., & Li, C. 2019,
913 *Advances in Space Research*, 63, 3404
914 **Zanetti, M., Stadermann, A., Jolliff, B., Hiesinger, H., van der Bogert, C.**
915 **H., & Plescia, J. 2017, *Icarus*, 298, 64**
916 Ziethe, R., Seiferlin, K., & Hiesinger, H. 2009, *Planet Space Sci*, 57, 784
917 Zhang, F., Zhu, M. H., Bugiolacchi, R., Huang, Q., Osinski, G. R., Xiao, L., &
918 Zou, Y. L. 2018, *Icarus*, 307, 216